Supporting Information for "Lagrangian versus Eulerian spectral estimates of surface kinetic energy over the global ocean"

Xinwen Zhang[1], Xiaolong Yu[1], Aurélien L. Ponte[2], Zoé Caspar-Cohen[2,3], Sylvie Le Gentil[2], Lu Wang[4,2], Wenping Gong[1]

[1]School of Marine Sciences, Sun Yat-sen University, and Southern Marine Science and Engineering Guangdong Laboratory (Zhuhai), Zhuhai, China

[2]Ifremer, Université de Brest, CNRS, IRD, Laboratoire d'Océanographie Physique et Spatiale, IUEM, Brest, France

[3]Scripps Institution of Oceanography, University of California, San Diego, La Jolla, California, USA

[4]Department of Mechanics and Engineering Science at College of Engineering, Peking University, Beijing, China

Contents of this file

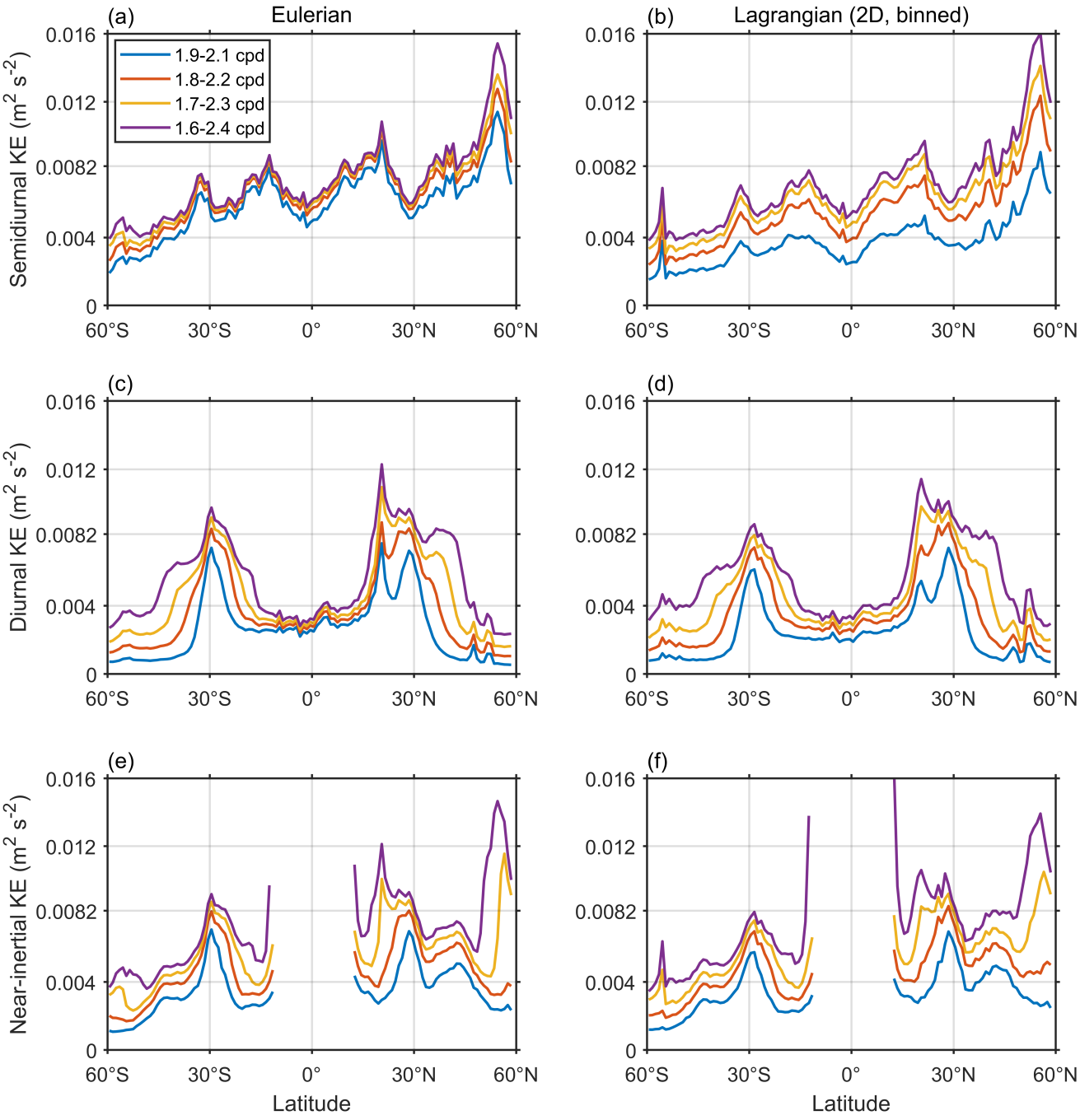

Figure S1. Zonally averaged (a, b) semidiurnal, (c, d) diurnal and (e, f) near-inertial KE in 1° latitude bins estimated from Eulerian velocity field (left panel) and Lagrangian particle trajectories with binning (right panel) at different bandwidths.

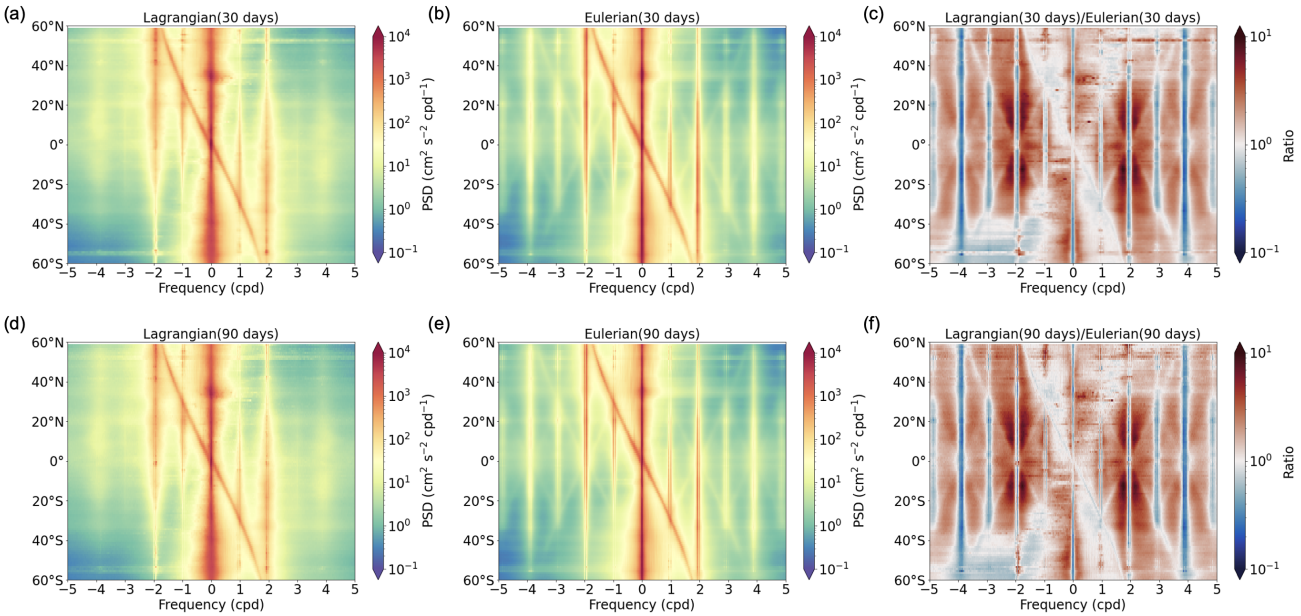

Figure S2. Zonally averaged rotary frequency spectra in 1° latitude bins from Lagrangian and Eulerian horizontal velocity fields at the surface layer and their ratio of (a, b, c) 30-day and (d, e ,f) 90-day segments, with positive (negative) frequencies corresponding to counterclockwise (clockwise) rotating motions, which are cyclonic (anticyclonic) in the Northern Hemisphere.

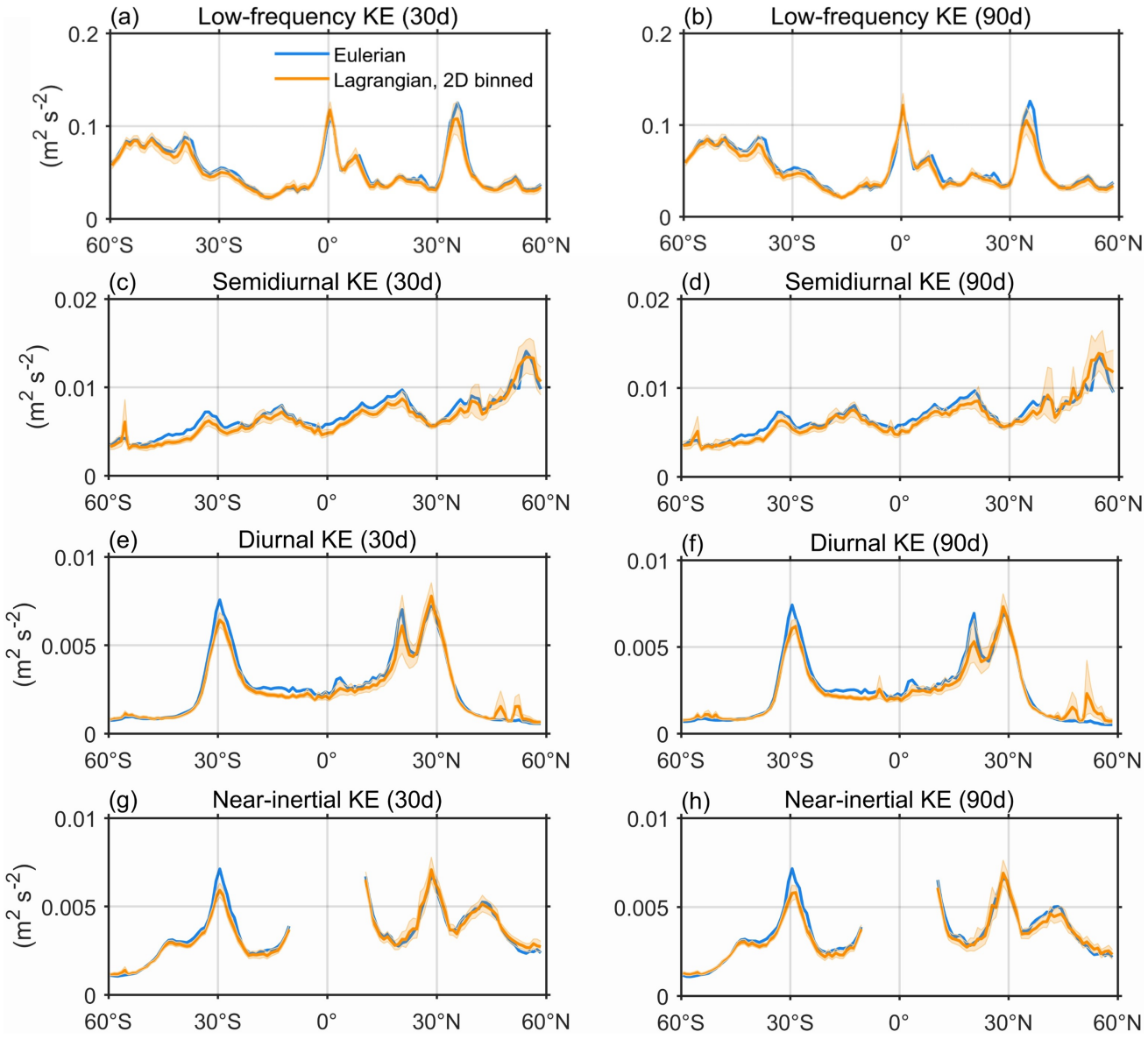

Figure S3. Zonally averaged (a, b) low-frequency, (c, d) semidiurnal, (e, f) near-inertial and (g, h) diurnal KE in 1° latitude bins estimated from Eulerian velocity field (blue) and Lagrangian particle trajectories with binning (orange). The left panels represent the results of 30-day segment, and the right panels represent the results of 90-day segment. The colored shading shows the 95% confidence interval determined using a bootstrapping resampling approach.

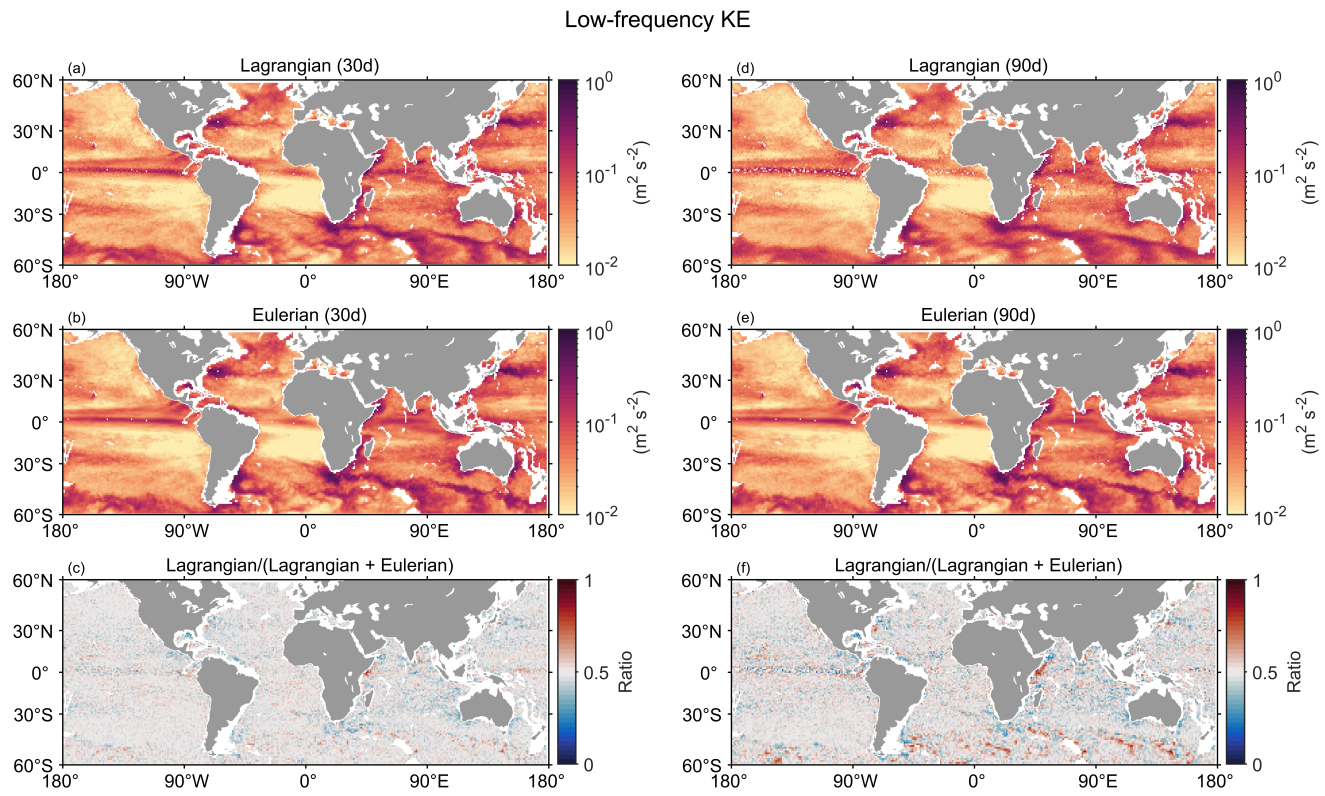

Figure S4. Global maps of Lagrangian and Eulerian low-frequency KE at the surface layer and the ratio of Lagrangian KE/(Lagrangian KE+Eulerian KE) in 1°× 1° bins of 30-day segment (left panel) and 90-day segment (right panel).

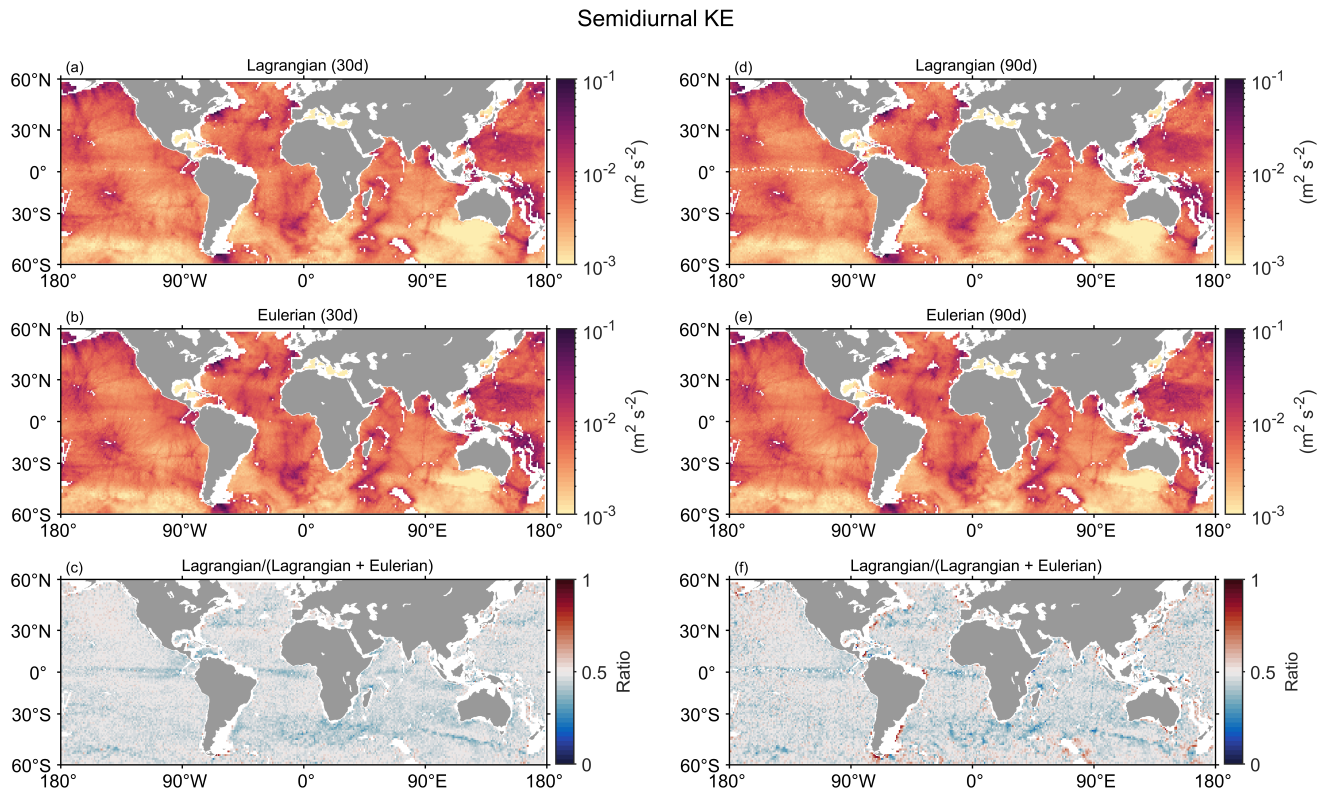

Figure S5. Global maps of Lagrangian and Eulerian semidiurnal KE at the surface layer and the ratio of Lagrangian KE/(Lagrangian KE+Eulerian KE) in 1°× 1° bins of 30-day segment (left panel) and 90-day segment (right panel).

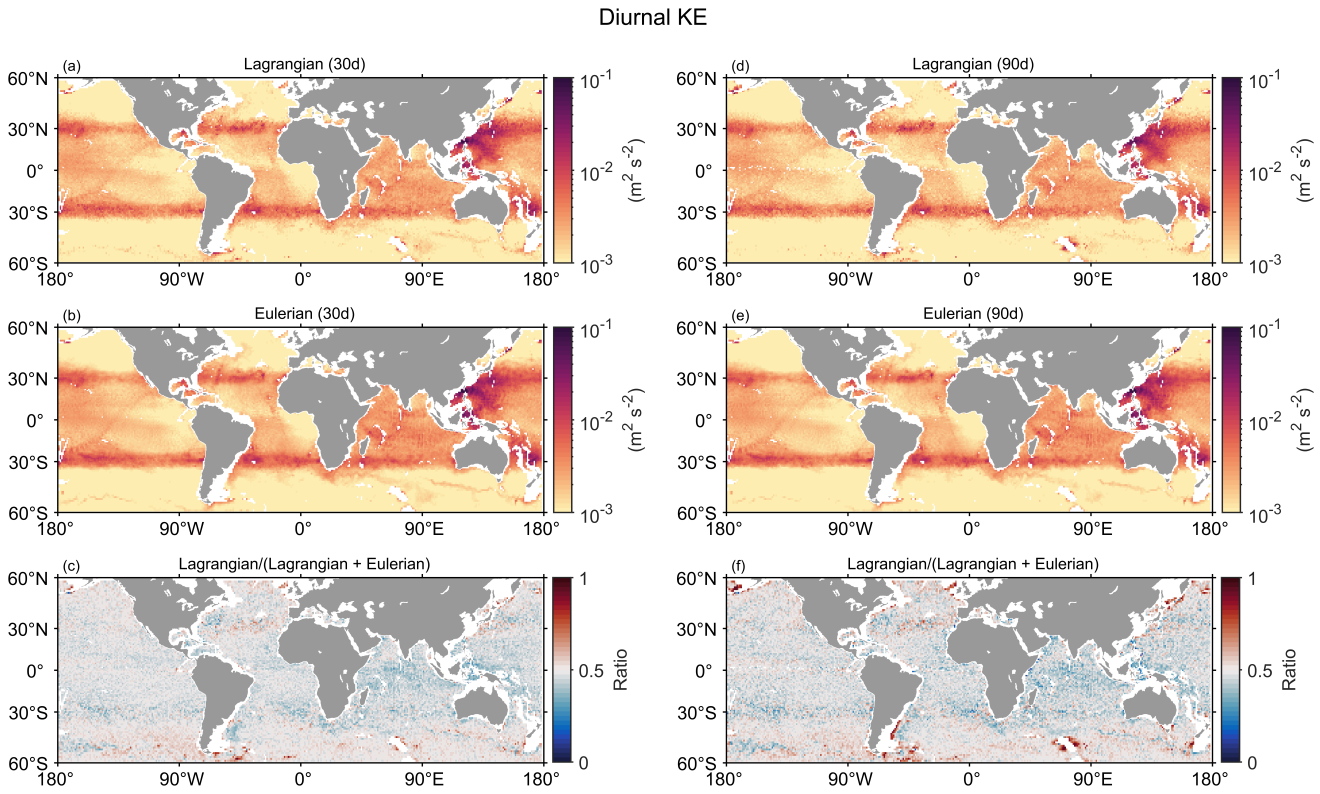

Figure S6. Global maps of Lagrangian and Eulerian diurnal KE at the surface layer and the ratio of Lagrangian KE/(Lagrangian KE+Eulerian KE) in 1°× 1° bins of 30-day segment (left panel) and 90-day segment (right panel).

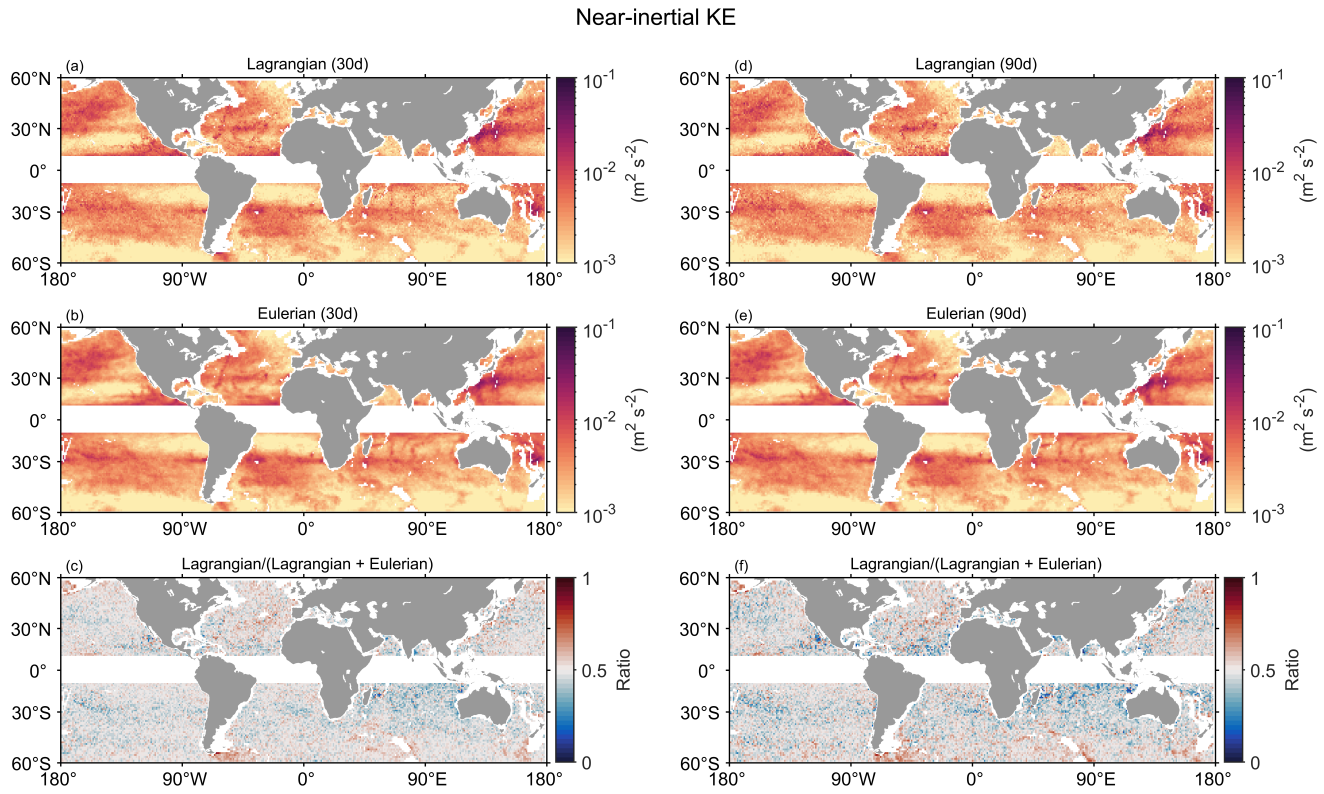

Figure S7. Global maps of Lagrangian and Eulerian near-inertial KE at the surface layer and the ratio of Lagrangian KE/(Lagrangian KE+Eulerian KE) in 1°× 1° bins of 30-day segment (left panel) and 90-day segment (right panel).